A cosmic origin of Venus' lower haze

Hiroki Karyu[1,2,3*], Takeshi Kuroda[1,4], Anni Määttänen[5], Arnaud Mahieux[2,6,7], Sébastien Viscardy[2], Naoki Terada[1], Séverine Robert[2], Ann Carine Vandaele[1,2], Michel Crucifix[3]

[1]Department of Geophysics, Graduate School of Science, Tohoku University, Sendai, Japan
[2]Royal Belgian Institute for Space Aeronomy, BIRA-IASB, Brussels, Belgium
[3]Earth and Life Institute, Université Catholique de Louvain, Louvain-la-Neuve, Belgium
[4]Division for the Establishment of Frontier Sciences of Organization for Advanced Studies, Tohoku University, Sendai, Japan
[5]LATMOS/IPSL, Sorbonne Université, UVSQ Université Paris-Saclay, CNRS, Paris, France
[6]The University of Texas at Austin, Austin, Texas
[7]Aurora Technology Services for the European Space Agency at ESAC, Madrid, Spain

*Corresponding author:
Hiroki Karyu
Graduate School of Science
Tohoku University
Sendai, Miyagi 980-8578, Japan
Email: hiroki.karyu.q4@dc.tohoku.ac.jp

Abstract

Unlike on Earth, where liquid droplets persist from the surface to the cloud tops[1], droplets on Venus evaporate in the hot lower atmosphere and never reach the surface[2]. Yet, entry probes have consistently revealed a layer containing involatile particles[3–5]—the lower haze—between Venus' surface and the main cloud deck. However, the origin of the lower haze layer has remained unknown since its discovery five decades ago. There has never been an attempt to reproduce the lower haze layer or investigate its origin in cloud modeling of Venus; instead, it has typically been treated as a given boundary condition[6–9]. Here we incorporate a self-consistent particle formation framework into a Venus cloud microphysics model and show, for the first time, that the continuous influx of cosmic dust is sufficient to sustain this lower haze layer with the particle size distribution observed by the entry probes. These haze particles of cosmic origin act as efficient condensation nuclei, promoting cloud formation in the main cloud deck even far from their initial source. Beyond this, these particles also provide a plausible source for the planet's long-unidentified ultraviolet absorber. Collectively, our findings establish cosmic dust as an essential component of Venus' climate. These insights are also crucial for understanding the climates of planets with thick atmospheres, such as gas giants and exoplanets, where accumulating cosmic dust can similarly affect the cloud structure and composition.

Main

Despite sharing a similar size and mass with Earth, Venus has a markedly different atmospheric composition and climate. Its atmosphere contains approximately 90 bars of carbon dioxide at the surface, resulting in an enhanced greenhouse effect that produces an extremely high temperature in the lower atmosphere[10,11]. Sulfuric acid (H_2SO_4) clouds—produced photochemically from sulfur dioxide (SO_2), carbonyl sulfide (OCS), and water (H_2O)—reside between 47 and 70 km (ref.[12,13]) and have a pivotal role in atmospheric radiative transfer[10,11], chemistry[14,15], and material transport[16,17]. Because H_2SO_4 cannot remain in the liquid phase in the intense heat of the lower atmosphere, any aerosol particles below this cloud deck would be expected to have non-sulfuric-acid composition.

For decades, entry probes from multiple missions—including those from the VeGa[5], Venera[4] missions, and Pioneer Venus (PV)[3]—have consistently detected an aerosol layer extending from the cloud base at ~47 km down to ~30 km, referred to as the lower haze layer[2]. The existence of the lower haze particles is also suggested by the analysis of near-infrared data taken by the Visible and Infrared Thermal Imaging Spectrometer (VIRTIS) onboard Venus Express (VEx)[18]. This indicates that Venus' clouds contain involatile substances other than sulfuric acid. The typical effective radius of the lower haze particles ranges from 0.08 (ref.[4]) to 0.21 μm (ref.[3]) and is thought to follow a lognormal distribution. These sub-cloud particles are transported upward into the main cloud deck, where they play a critical role in cloud formation by acting as cloud condensation nuclei (CCN)[7,19,20].

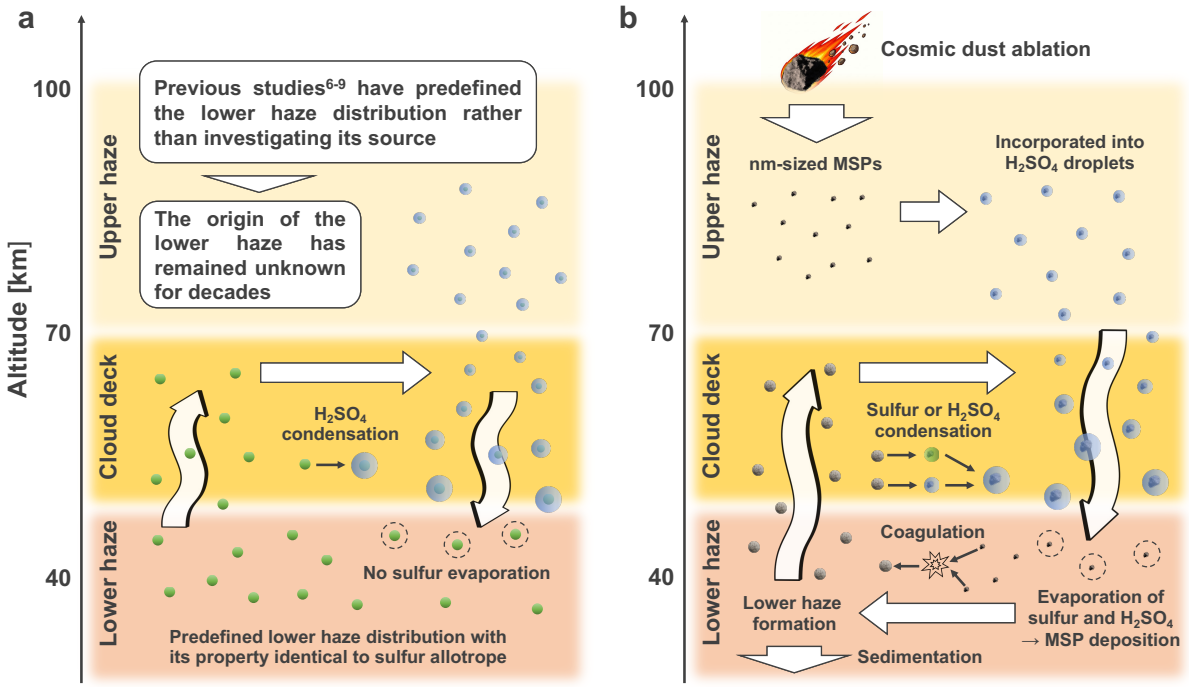

Fig. 1 | Cloud cycle on Venus. a, Sketch of the cloud cycle on Venus simulated by previous microphysics models[6–9] with predefined lower haze distribution. **b**, Sketch of the cloud cycle on Venus simulated by this study with the meteoric smoke particle (MSP) injection and the subsequent lower haze formation.

However, despite its importance for cloud formation processes, the origin and composition of the lower haze have remained an enduring mystery. All previous cloud microphysics models have imposed the lower haze particle population as a boundary condition in order to reproduce the observed cloud profile[6–9] (Fig. 1a). For simplicity, it has also been assumed that these particles are composed of either an unknown involatile material or sulfur allotropes. Sulfur allotropes can be regarded as volatile in Venus' atmospheric conditions. However, whether sulfur allotropes can remain in the solid phase below the cloud base is uncertain, because their condensation and evaporation are not included in the current cloud microphysics models[7,8]. As a result, no self-consistent model—one that simulates both the haze's formation from its source and its interaction with cloud droplets—has yet to be developed, leaving its origin unexplained.

Here, we demonstrate that cosmic dust can provide the crucial source for Venus' lower haze layer through self-consistent cloud microphysics simulations, finally providing an explanation of its composition and formation. Our model incorporates nucleation and condensation

of three key condensable vapor species—H_2SO_4, water (H_2O), and sulfur allotrope (S_8)—to model particle formation and their evolution without relying on prescribed lower haze particle size distribution at the bottom boundary (see Methods). Furthermore, our model includes the injection of meteoric smoke particles (MSPs), which originate from the ablation of cosmic dust particles[21,22], as a source of the involatile particle component (see Methods). The injection rate is scaled by the cosmic dust ablation flux, whose typical value is estimated at ~10 tons day^{-1} (ref.[23]). However, the cosmic dust ablation flux on Venus is highly uncertain, as even Earth's estimate remains uncertain by approximately an order of magnitude. Therefore, we conducted a comprehensive parameter sensitivity analysis by varying the MSP influx between 0 and 1000 tons day^{-1}.

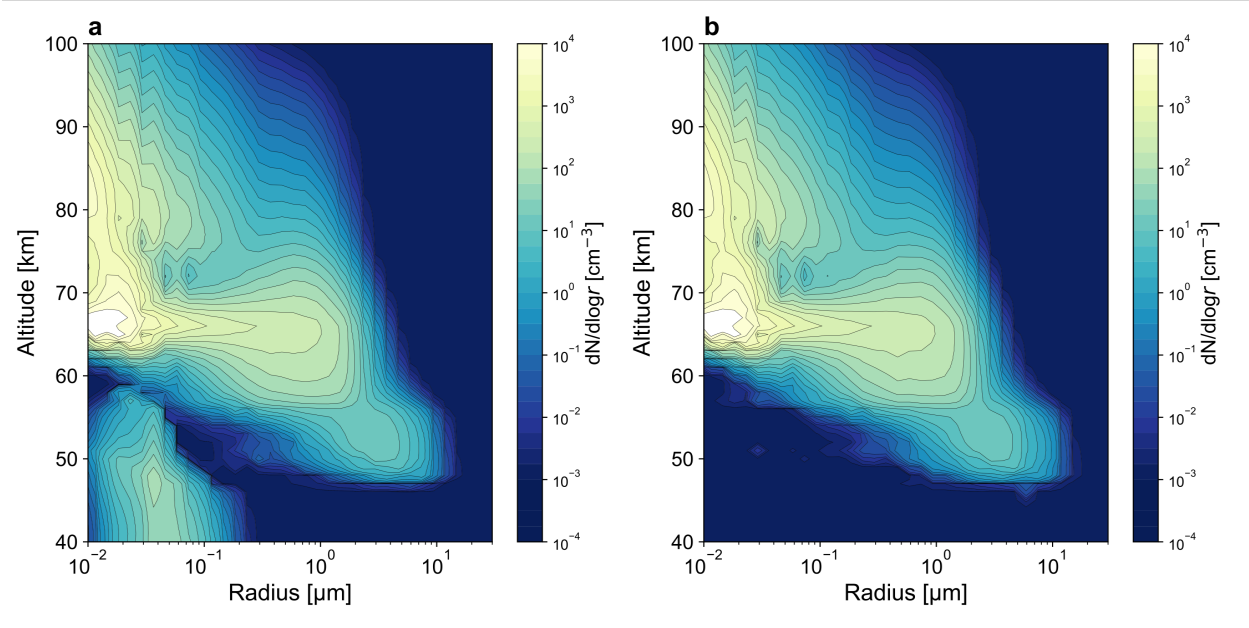

Fig. 2 | The lower haze formation under the cloud deck of Venus. a, b, Steady-state size distributions of aerosols as a function of particle radius (μm) and altitude (km) obtained from the microphysics simulations with (**a**) MSP influx of 10 tons day^{-1} and (**b**) without MSP influx.

The importance of MSP influx in the formation of the lower haze layer is clearly demonstrated. Indeed, the lower haze forms only when MSP influx is included in the simulation (Fig. 2a), and a sulfur haze does not form under the cloud base in either case. MSPs injected at the top of the atmosphere are scavenged by sulfuric acid aerosols at high altitudes and descend through the main cloud deck (Fig. 1b). Upon reaching the cloud bottom, the sulfuric acid evaporates,

leaving behind involatile residues originally carried by the MSPs. In contrast, when the MSP influx is not included, the lower haze does not form (Fig. 2b). Furthermore, our self-consistent modeling of particle formation reveals that sulfur allotrope particles are not stable in the solid phase below the cloud base. This finding raises questions about previous modeling approaches[6–9] in which CCN are predefined at the bottom boundary and assumed to be microphysically equivalent to solid sulfur allotrope particles.

We investigated whether sources of other substances other than MSP could generate the lower haze. One possibility is volcanic ash or surface dust. However, even assuming fluxes several orders of magnitude greater than the MSP influx and adopting optimistic transport efficiencies, our results show that these sources cannot reproduce the lower haze characteristics (Supplementary Information, Section S1). Another possibility is photochemically produced species—for example, sulfur allotropes not considered in this study and carbonyl disulfide. However, these species do not condense under lower-haze conditions (Supplementary Information, Section S2).

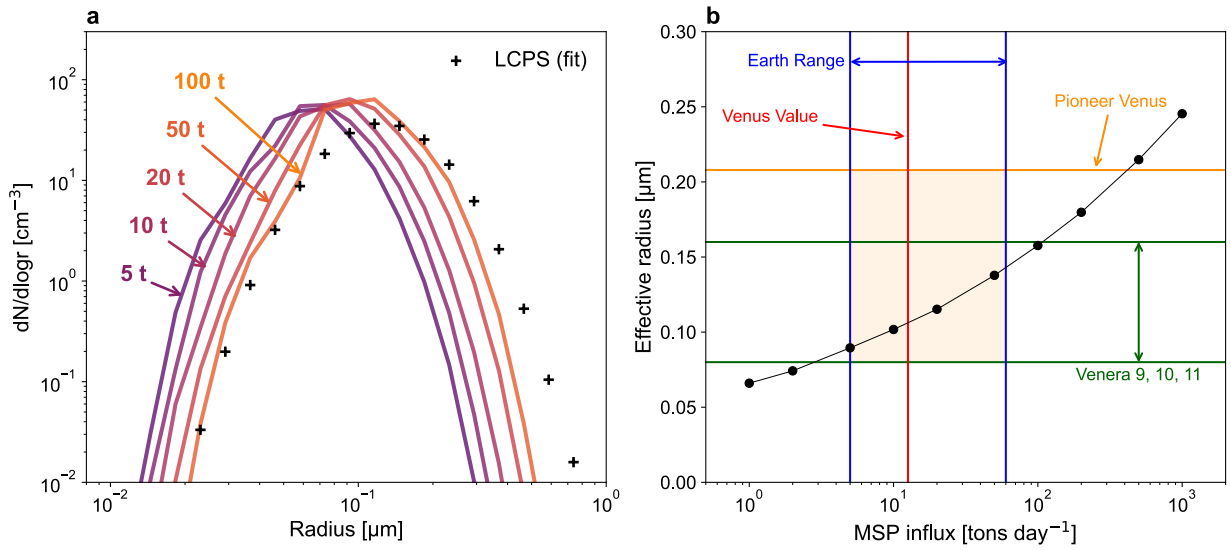

Fig. 3 | The dependence of the lower haze particle size on MSP influx. a, Steady-state size distribution of the lower haze particles at the altitude of 40 km obtained from the microphysics simulations with MSP influxes ranging from 5 to 100 tons day^{-1}. The corresponding fluxes are indicated by the colored arrows. The black cross indicates the size distribution estimated from the LCPS measurements[3]. **b**, Effective radius of the lower haze particles at 40 km calculated as a function of MSP influx. The red and blue lines indicate the estimated MSP influx on Venus[23] and the uncertainty range of MSP influx on Earth[25,26], respectively. The orange and green lines indicate the effective radius measured by the LCPS[3] and the range of effective radius measured by Venera 9, 10, and 11 probes[4], respectively. The yellow-shaded area indicates the parameter range that satisfies both the observed effective radii and the uncertainty range of MSP influx.

The resulting aerosol size distribution at 40 km closely resembles a lognormal distribution (Fig. 3) and is, in all cases, qualitatively consistent with that inferred from measurements by the Cloud Particle Size Spectrometer onboard the PV Large Probe (LCPS)[3] in all cases. We also confirmed that particle source from below, such as volcanic ash, does not produce a lognormal distribution by itself (Supplementary Information S1). Although the lower haze number density is an estimated value, it serves as a reliable reference because cloud microphysics models using this number density as a bottom boundary condition have consistently reproduced observed cloud properties[6–8,20]. The total haze number density agrees with the LCPS observations within a factor of two in all MSP influx scenarios, with the mode radius increasing with influx.

The final mode radius of the lower haze is governed by a multi-stage process that begins in the upper atmosphere, as illustrated in Fig. 1b. First, incoming 1-nm MSPs are primarily incorporated into pre-existing sulfuric acid aerosols in the upper haze layer. An increase in the MSP influx does not create more particles but rather increases the mass of involatile material within each mixed haze particle. As these mixed particles sediment and cross the cloud base, sulfuric acid evaporates due to high temperature. This process releases the involatile MSP material, and the residual cores are now larger than the initial 1-nm MSPs. Higher initial MSP influxes lead to larger residual cores being released below the clouds. Finally, this population of enlarged, newly released particles accumulate and coagulate, forming the lower haze. The ultimate particle size is determined by a steady state balancing between the mass influx of these residual cores from above and their removal by sedimentation. Consequently, a greater initial MSP influx results in larger cores being released, which in turn coagulate into a lower haze with a larger mode radius.

We converted the modeled size distribution into the effective radius, defined as an area-weighted mean radius[1], to enable direct comparison with past probe measurements[3,4] (Fig. 3b). Observations of the lower haze particles report a range of effective radii. The nephelometer and onboard Venera 9 reported particle radii between 0.08 and 0.16 μm[4]. For Venera 10, the nephelometer recorded significantly higher backscatter, which was attributed to either an increased particle abundance or a shift in the size distribution[4]. Venera 11 did not detect lower haze particles with the nephelometer[4], whereas the spectrophotometer data indicated their presence and reported particle radii between 0.08 and 0.1 μm (ref. [27]). Collectively, measurements from the Venera 9, 10, and 11 probes suggest a working range of 0.08 to 0.16 μm. On the other hand, the Pioneer Venus LCPS instrument reported a larger value of 0.21 μm (ref. [3]). This discrepancy may arise because the PV LCPS value was not measured directly but was instead estimated from a limited number of data points near the instrument's detection limit. In fact, Knollenberg and Hunten[3] stated that the particle population around ~0.1 μm is "only first-order refinements with an admitted large uncertainty." Given the scarcity and uncertainties in these observations, we adopt a working range for the lower haze effective radius of 0.08 to 0.21 μm. The corresponding MSP influx required to satisfy this condition ranges from approximately 3 to 300 tons day^{-1}. Since the MSP influx on Venus remains highly uncertain, this influx range can be further constrained by referencing Earth's values as a strong benchmark for a realistic rate. The lower limit of ablation flux, estimated from Earth's sodium layer measurements, is around 5 tons day^{-1} (ref.[24,26]). while the upper limit flux

before ablation is approximately 60 tons day^{-1} (ref. [23,28]). This range also encompasses the typically estimated Venus' value of about 12 tons day^{-1} (ref.[23]). The significant overlap suggests that the observed characteristics of Venus' lower haze can be explained by a realistic MSP influx common to terrestrial planets.

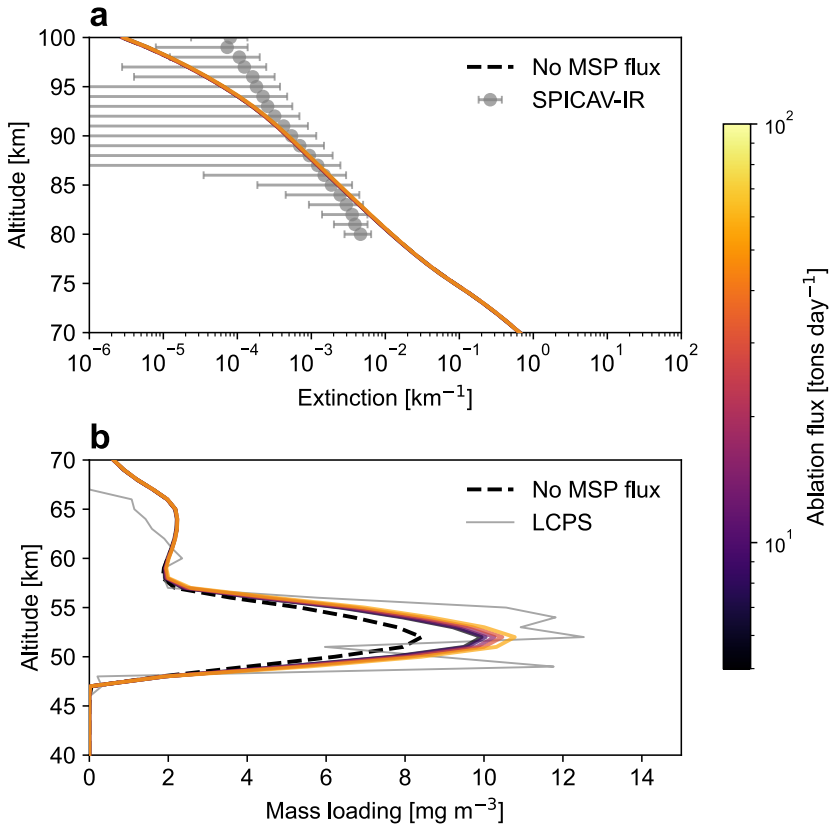

Fig. 4 | The dependence of the cloud structure on MSP influx. a, Steady-state aerosol extinction profiles at 1 μm wavelength obtained from the microphysics simulations with MSP fluxes ranging from 5 to 100 tons day^{-1}. All the curves are nearly indistinguishable, as their values are approximately the same. The grey circles and error bars indicate observed aerosol extinction at ~1 μm derived from the Spectroscopy for Investigation of Characteristics of the Atmosphere of Venus (SPICAV) data onboard VEx[29]. **b**, Steady-state aerosol mass loading profiles obtained from the microphysics simulations with MSP influxes ranging from 5 to 100 tons day^{-1}. The grey line indicates the mass loading measured by PV LCPS[3]. Note that an off-scale mass loading data point from the LCPS data, approximately 90 mg m^{-3} and peaking around 49 km, is not displayed in the figure for readability.

The MSP influx significantly impacts cloud formation in the main cloud deck (Fig. 4). The lower haze particles, formed from MSPs, are transported upward by eddy diffusion, where they act as efficient CCN for H_2SO_4-H_2O droplets. This seeding process substantially increases the total cloud mass loading, with a higher influx resulting in a greater cloud mass (Fig. 4b). The particle size is an important factor. A higher influx produces larger haze particles which, due to the Kelvin effect[1], require less supersaturation to become cloud droplets. For instance, compared to the no-MSP case, a 5 tons day^{-1} MSP influx increases mass loading by 18%, while 100 tons day^{-1} results in a 28% increase. This enhancement brings simulations into closer agreement with the LCPS observations[3] (Fig. 4b), highlighting the substantial impact of MSP-enhanced cloud formation.

In contrast, MSP influx has a negligible effect on the upper haze formation (Fig. 4a). Cloud formation at these altitudes can be affected by two-component homogeneous nucleation of H_2SO_4-H_2O and homogeneous nucleation of sulfur allotrope, rather than by heterogeneous nucleation on MSPs. This small contribution of MSPs does not significantly alter the particle size distribution in the upper haze, consistent with a prior modeling study[9]. Overall, the influence of MSP influx on cloud structure is somewhat counterintuitive: it primarily affects the main cloud deck—far from its initial source—rather than the upper haze at higher altitudes, which is closer to the source.

The shape of the lower haze particles may have an impact on their atmospheric abundance. While the current model assumes a spherical geometry, the coagulation of solid particles may lead to the formation of fractal aggregate structures. Compared to their spherical particles, aggregate particles exhibit higher coagulation efficiencies and lower sedimentation velocities, due to their morphology[1]. The combined result of these properties would be an enhanced mass loading, as particles can grow larger while maintaining a reduced sedimentation velocity. Consequently, the mass loading of the lower haze calculated in this study should be viewed as a lower limit for each respective influx scenario.

Our results suggest that the lower haze particles can provide a source for the mysterious UV-blue absorber on Venus[30]. The MSPs introduce various involatile species into Venus' atmosphere, including iron (Fe), magnesium (Mg), and silicon (Si). These species can then accumulate as lower haze particles (Extended Data Table 1). This accumulation of iron provides an explanation for the iron detected by both the VEGA and Venera probes[31]. Furthermore, recent reanalysis of the mass spectrometer onboard the PV Large Probe indicates that iron sulfate is

present in the cloud droplets, likely explained by the inclusion of cosmic material[32]. The present study aligns with this observation. Iron compounds have long been proposed as candidates for the unknown UV-blue absorber on Venus[33]. Specifically, proposed mechanisms include iron chloride forming from reactions with hydrogen chloride[34–36], or iron sulfates forming in H_2SO_4-H_2O droplets, which has been proposed by a recent study[37]. If the haze particles existing between 40 and 57 km, which is prevented from condensation due to their high heterogeneous nucleation barrier (Fig. 2a), are transported by cloud-penetrative convection[38,39] and incorporated into H_2SO_4 aerosols, the UV-blue absorption feature can form at the cloud top. This scenario aligns with the previous observations, suggesting that the UV-blue absorber is hidden beneath the upper cloud and transported convectively from the layer below[40,41]. Thus, our work provides the crucial missing link between observational and experimental studies of the UV absorber by identifying a viable physical source of the iron.

Our findings show that MSPs are critical to Venus' climate, operating through two primary mechanisms. First, MSPs strengthen the planet's greenhouse effect by enhancing the main cloud deck and trapping outgoing thermal radiation[10,11]. Given the atmosphere's low stability between 50 and 60 km, even a slight change in the heating rate can readily destabilize the cloud layer[10]. The subsequent heating at the cloud base drives strong convection in this altitude range, which further contributes to cloud formation, consequently creating a positive feedback loop[20]. Second, the MSPs provide iron compounds, which can serve as a UV absorber in the Venusian atmosphere[30]. In fact, half of the incident solar energy is deposited between 57 and 70 km and causes strong heating, which stabilizes the atmosphere above 60 km[10]. This heating excites thermal tides and maintains the atmospheric super-rotation that effectively transports heat from the dayside to the nightside[42]. Collectively, these effects originating from MSPs potentially affect the radiative budget of Venus' atmosphere by influencing both outgoing thermal and incoming solar radiation, and thus, its climate.

The upcoming missions will offer the opportunity to investigate the characteristics of the lower haze layer in greater detail. In particular, the Venus Mass Spectrometer (VMS) on DAVINCI is designed to detect compounds across a broad mass range, from 2 to 550 Da (ref.[43]). The masses of gaseous species that would sublimate from MSP-related compounds fall within this detectable range, which would provide direct evidence of their composition and abundance. More specifically, the potential for detecting iron as iron chloride is noteworthy, as its abundance in the gas phase is

predicted to reach up to 17 ppb due to sublimation from the solid phase[35]. The detection of such species by VMS will be crucial for confirming the origin of the lower haze layer and assessing its potential as a UV-blue absorber.

To better constrain the MSP influx, we recommend targeted observations of metal layers—such as sodium (Na), Mg, and Fe—in the Venus atmosphere. These layers could be characterized by detecting the ultraviolet-visible emissions unique to these species[26]. On Earth, the MSP influx is typically estimated by comparing observed metal species distributions with those generated in numerical simulations[23,24,26,28]. Adopting a similarly integrated approach will be essential for narrowing the MSP influx range presented in Fig. 3b and for refining our understanding of the resulting lower haze properties.

Finally, we discuss the implications of our findings for other planets. While the well-studied upper hazes on solar system gas giants are composed of organic photochemistry products, the microphysical processes below the main cloud decks are poorly understood, particularly regarding the origin and composition of CCN[44]. On these planets, involatile particles are likely not effectively scavenged from the atmosphere because, similar to Venus, cloud particles eventually evaporate completely below the cloud base[45]. Equilibrium cloud condensation models predict that water cloud droplets form near the cloud base on Jupiter, Saturn, and Neptune, where atmospheric temperatures exceed ~300 K (ref.[45]). At such high temperatures, water cannot efficiently nucleate on its own and thus requires pre-existing CCN. Significant cosmic dust injection has been estimated on gas giants[46,47]. Drawing from our Venus simulations, the cosmic dust ablation would lead to the formation of sub-micron particle layers below the cloud base. These sub-micron particles deposited under the cloud deck would be transported upward again by vigorous convection and contribute to water droplet formation[48]. This mechanism should be particularly important for Jupiter, which is estimated to receive an even greater flux of cosmic dust ablation than Venus[47]. Similarly to Venus, observing the metal layers of the outer planets would help constrain the deposition rates of Na, Mg, and Fe within their atmospheres, as well as the resulting haze abundances. Ideally, in-situ probe measurements—analogous to those performed by the Pioneer Venus LCPS—would be pivotal for characterizing the lower haze particles beneath the primary cloud decks of these giant planets.

On planets like Earth, where surface liquid water exists, rain constantly scavenges involatile particles from the air[1]. However, as observed in our Solar System, planets with surface

liquid water are truly unique; most planets possess dry atmospheres where liquid droplets evaporate before reaching the surface[49]. In such worlds, the lower haze originating from cosmic dust can accumulate in the hot lower atmosphere, enhancing cloud formation by acting as efficient CCN, as illustrated in Fig. 1b. This would significantly impact the planet's climate, as clouds exhibit a strong radiative effect[50]. Furthermore, iron compounds within the cloud particles can alter their optical properties, including UV light absorption[37]. These effects establish cosmic dust as an essential component of planetary climates, a role that is also likely to be significant for exoplanets.

References

1. Pruppacher, H. R. & Klett, J. D. *Microphysics of Clouds and Precipitation*. (Springer Netherlands Springer e-books, Dordrecht, 2010).
2. Titov, D. V., Ignatiev, N. I., McGouldrick, K., Wilquet, V. & Wilson, C. F. Clouds and Hazes of Venus. *Space Sci Rev* **214**, 126 (2018).
3. Knollenberg, R. G. & Hunten, D. M. The microphysics of the clouds of Venus: Results of the Pioneer Venus Particle Size Spectrometer Experiment. *J. Geophys. Res.* **85**, 8039–8058 (1980).
4. Marov, M. Ya., Lystsev, V. E., Lebedev, V. N., Lukashevich, N. L. & Shari, V. P. The structure and microphysical properties of the Venus clouds: Venera 9, 10, and 11 data. *Icarus* **44**, 608–639 (1980).
5. Gnedykh, V. I., Zasova, L. V., Moroz, V. I., Moshkin, B. E. & Ekonomov, A. P. The vertical structure of the Venus cloud layer at the landing sites of Vega 1 and Vega 2. *Kosmicheskie Issledovaniia* **25**, 707–714 (1987).
6. Imamura, T. & Hashimoto, G. L. Microphysics of Venusian Clouds in Rising Tropical Air. *J. Atmos. Sci.* **58**, 3597–3612 (2001).
7. McGouldrick, K. & Barth, E. L. The Influence of Cloud Condensation Nucleus Coagulation on the Venus Cloud Structure. *Planet. Sci. J.* **4**, 50 (2023).
8. Karyu, H. *et al.* One-dimensional Microphysics Model of Venusian Clouds from 40 to 100 km: Impact of the Middle-atmosphere Eddy Transport and SOIR Temperature Profile on the Cloud Structure. *Planet. Sci. J.* **5**, 57 (2024).
9. Gao, P., Zhang, X., Crisp, D., Bardeen, C. G. & Yung, Y. L. Bimodal distribution of sulfuric acid aerosols in the upper haze of Venus. *Icarus* **231**, 83–98 (2014).
10. Limaye, S. S. *et al.* Venus Atmospheric Thermal Structure and Radiative Balance. *Space Sci Rev* **214**, 102 (2018).

11. Haus, R. *et al.* Radiative energy balance of Venus based on improved models of the middle and lower atmosphere. *Icarus* **272**, 178–205 (2016).
12. Yung, Y. L. & Demore, W. B. Photochemistry of the stratosphere of Venus: Implications for atmospheric evolution. *Icarus* **51**, 199–247 (1982).
13. Krasnopolsky, V. A. S3 and S4 abundances and improved chemical kinetic model for the lower atmosphere of Venus. *Icarus* **225**, 570–580 (2013).
14. Krasnopolsky, V. A. & Pollack, J. B. H2O-H2SO4 System in Venus' Clouds and OCS, CO, and H2SO4 Profiles in Venus' Troposphere. *Icarus* **109**, 58–78 (1994).
15. Ubukata, S. *et al.* Uptake of SO_2 into Sulfuric Acid Droplets through the Oxidation by NO_2 under Venus-Analogous Conditions. *ACS Earth Space Chem.* **9**, 1525–1533 (2025).
16. Karyu, H. *et al.* Vertical-Wind-Induced Cloud Opacity Variation in Low Latitudes Simulated by a Venus GCM. *JGR Planets* **128**, e2022JE007595 (2023).
17. Stolzenbach, A., Lefèvre, F., Lebonnois, S. & Määttänen, A. Three-dimensional modeling of Venus photochemistry and clouds. *Icarus* **395**, 115447 (2023).
18. Satoh, T. *et al.* Cloud structure in Venus middle-to-lower atmosphere as inferred from VEX/VIRTIS 1.74 μ m data. *J. Geophys. Res.* **114**, 2008JE003184 (2009).
19. McGouldrick, K. Effects of variation in coagulation and photochemistry parameters on the particle size distributions in the Venus clouds. *Earth Planets Space* **69**, 161 (2017).
20. McGouldrick, K. & Toon, O. An investigation of possible causes of the holes in the condensational Venus cloud using a microphysical cloud model with a radiative-dynamical feedback. *Icarus* **191**, 1–24 (2007).
21. Hunten, D. M., Turco, R. P. & Toon, O. B. Smoke and Dust Particles of Meteoric Origin in the Mesosphere and Stratosphere. *J. Atmos. Sci.* **37**, 1342–1357 (1980).

22. Murray, Benjamin. J., Mangan, Thomas. P., Määttänen, A. & Plane, John. M. C. Ephemeral Ice Clouds in the Upper Mesosphere of Venus. *JGR Planets* **128**, e2023JE007974 (2023).
23. Carrillo-Sánchez, J. D. *et al.* Cosmic dust fluxes in the atmospheres of Earth, Mars, and Venus. *Icarus* **335**, 113395 (2020).
24. Marsh, D. R., Janches, D., Feng, W. & Plane, J. M. C. A global model of meteoric sodium. *JGR Atmospheres* **118**, (2013).
25. Lanci, L., Kent, D. V. & Biscaye, P. E. Meteoric smoke concentration in the Vostok ice core estimated from superparamagnetic relaxation and some consequences for estimates of Earth accretion rate. *Geophysical Research Letters* **34**, 2007GL029811 (2007).
26. Plane, J. M. C., Feng, W. & Dawkins, E. C. M. The Mesosphere and Metals: Chemistry and Changes. *Chem. Rev.* **115**, 4497–4541 (2015).
27. Moroz, V. I., Ekonomov, A. P., Golovin, Yu. M., Moshkin, B. E. & San'ko, N. F. Solar radiation scattered in the Venus atmosphere: The Venera 11,12 data. *Icarus* **53**, 509–537 (1983).
28. Gardner, C. S., Liu, A. Z., Marsh, D. R., Feng, W. & Plane, J. M. C. Inferring the global cosmic dust influx to the Earth's atmosphere from lidar observations of the vertical flux of mesospheric Na. *JGR Space Physics* **119**, 7870–7879 (2014).
29. Luginin, M. *et al.* Bimodal aerosol distribution in Venus' upper haze from joint SPICAV-UV and -IR observations on Venus Express. *Icarus* **409**, 115866 (2024).
30. Pollack, J. B. *et al.* Distribution and source of the UV absorption in Venus' atmosphere. *J. Geophys. Res.* **85**, 8141–8150 (1980).
31. Krasnopolsky, V. A. Vega mission results and chemical composition of Venusian clouds. *Icarus* **80**, 202–210 (1989).

32. Mogul, R., Zolotov, M. Yu., Way, M. J. & Limaye, S. S. Re-Analysis of Pioneer Venus Data: Water, Iron Sulfate, and Sulfuric Acid are Major Components in Venus' Aerosols. *JGR Planets* **130**, e2024JE008582 (2025).
33. Zasova, L. V., Krasnopolsky, V. A. & Moroz, V. I. Vertical distribution of SO2 in upper cloud layer of Venus and Origin of U.V.-absorption. *Advances in Space Research* **1**, 13–16 (1981).
34. Krasnopolsky, V. A. Chemical composition of venus clouds. *Planetary and Space Science* **33**, 109–117 (1985).
35. Krasnopolsky, V. A. On the iron chloride aerosol in the clouds of Venus. *Icarus* **286**, 134–137 (2017).
36. Egan, J. V., James, A. D. & Plane, J. M. C. Laboratory Measurements of Ferric Chloride ($FeCl_3$) under Venusian Conditions. *ACS Earth Space Chem.* **9**, 2127–2136 (2025).
37. Jiang, C. Z. *et al.* Iron-sulfur chemistry can explain the ultraviolet absorber in the clouds of Venus. *Sci. Adv.* **10**, eadg8826 (2024).
38. Baker, R. D., Schubert, G. & Jones, P. W. High Rayleigh number compressible convection in Venus' atmosphere: Penetration, entrainment, and turbulence.
39. Lefèvre, M., Marcq, E. & Lefèvre, F. The impact of turbulent vertical mixing in the Venus clouds on chemical tracers. *Icarus* **386**, 115148 (2022).
40. Titov, D. V. *et al.* Atmospheric structure and dynamics as the cause of ultraviolet markings in the clouds of Venus. *Nature* **456**, 620–623 (2008).
41. Titov, D. V. *et al.* Morphology of the cloud tops as observed by the Venus Express Monitoring Camera. *Icarus* **217**, 682–701 (2012).
42. Horinouchi, T. *et al.* How waves and turbulence maintain the super-rotation of Venus' atmosphere. *Science* **368**, 405–409 (2020).

43. Garvin, J. B. *et al.* Revealing the Mysteries of Venus: The DAVINCI Mission. *Planet. Sci. J.* **3**, 117 (2022).
44. Yair, Y., Levin, Z. & Tzivion, S. Microphysical Processes and Dynamics of a Jovian Thundercloud. *Icarus* **114**, 278–299 (1995).
45. Atreya, S. K. & Wong, A.-S. Coupled Clouds and Chemistry of the Giant Planets— A Case for Multiprobes. *Space Sci Rev* **116**, 121–136 (2005).
46. Moses, J. I. & Poppe, A. R. Dust ablation on the giant planets: Consequences for stratospheric photochemistry. *Icarus* **297**, 33–58 (2017).
47. Poppe, A. R. An improved model for interplanetary dust fluxes in the outer Solar System. *Icarus* **264**, 369–386 (2016).
48. Sugiyama, K., Nakajima, K., Odaka, M., Kuramoto, K. & Hayashi, Y.-Y. Numerical simulations of Jupiter's moist convection layer: Structure and dynamics in statistically steady states. *Icarus* **229**, 71–91 (2014).
49. Sánchez-Lavega, A., Pérez-Hoyos, S. & Hueso, R. Clouds in planetary atmospheres: A useful application of the Clausius–Clapeyron equation. *American Journal of Physics* **72**, 767–774 (2004).
50. Pierrehumbert, R. T. *Principles of Planetary Climate*. (Cambridge University Press, 2010). doi:10.1017/CBO9780511780783.
51. Karyu, H. *et al.* A Microphysics Model of Multicomponent Venus' Clouds With a High-Accuracy Condensation Scheme. *Earth and Space Science* **12**, e2025EA004203 (2025).
52. Jacobson, M. Z. *Fundamentals of Atmospheric Modeling, Second Edition*.
53. Krasnopolsky, V. A. A photochemical model for the Venus atmosphere at 47–112km. *Icarus* **218**, 230–246 (2012).

54. Zhang, X., Liang, M. C., Mills, F. P., Belyaev, D. A. & Yung, Y. L. Sulfur chemistry in the middle atmosphere of Venus. *Icarus* **217**, 714–739 (2012).
55. Steudel, R., Steudel, Y. & Wong, M. W. Speciation and Thermodynamics of Sulfur Vapor. in *Elemental Sulfur and Sulfur-Rich Compounds I* (ed. Steudel, R.) vol. 230 117–134 (Springer Berlin Heidelberg, Berlin, Heidelberg, 2003).
56. Lyons, J. R. An estimate of the equilibrium speciation of sulfur vapor over solid sulfur and implications for planetary atmospheres. *Journal of Sulfur Chemistry* **29**, 269–279 (2008).
57. Määttänen, A. *et al.* New Parameterizations for Neutral and Ion-Induced Sulfuric Acid-Water Particle Formation in Nucleation and Kinetic Regimes. *JGR Atmospheres* **123**, 1269–1296 (2018).
58. Onischuk, A. A. *et al.* Surface tension of sulfur nanoparticles as determined from homogeneous nucleation experiments. *Journal of Aerosol Science* **97**, 1–21 (2016).
59. Saunders, R. W. & Plane, J. M. C. A laboratory study of meteor smoke analogues: Composition, optical properties and growth kinetics. *Journal of Atmospheric and Solar-Terrestrial Physics* **68**, 2182–2202 (2006).
60. Frankland, V. L. *et al.* CO oxidation and O2 removal on meteoric material in Venus' atmosphere. *Icarus* **296**, 150–162 (2017).
61. Inada, A. Simulations of Martian surface fog and calibration of Mars Imaging Camera for its future observations. (Kobe University, Kobe, Japan, 2002).
62. Määttänen, A. *et al.* Nucleation studies in the Martian atmosphere. *J. Geophys. Res.* **110**, 2004JE002308 (2005).
63. Toon, O. B., Turco, R. P. & Pollack, J. B. The ultraviolet absorber on Venus: Amorphous sulfur. *Icarus* **51**, 358–373 (1982).

64. Seiff, A. *et al.* Models of the structure of the atmosphere of Venus from the surface to 100 kilometers altitude. *Advances in Space Research* **5**, 3–58 (1985).

65. Arney, G. *et al.* Spatially resolved measurements of H_2O, HCl, CO, OCS, SO_2, cloud opacity, and acid concentration in the Venus near-infrared spectral windows: MEASUREMENTS OF VENUS LOWER ATMOSPHERE. *J. Geophys. Res. Planets* **119**, 1860–1891 (2014).

66. Bézard, B., Fedorova, A., Bertaux, J.-L., Rodin, A. & Korablev, O. The 1.10- and 1.18-μm nightside windows of Venus observed by SPICAV-IR aboard Venus Express. *Icarus* **216**, 173–183 (2011).

67. Fedorova, A., Bézard, B., Bertaux, J.-L., Korablev, O. & Wilson, C. The CO2 continuum absorption in the 1.10- and 1.18-μm windows on Venus from Maxwell Montes transits by SPICAV IR onboard Venus express. *Planetary and Space Science* **113–114**, 66–77 (2015).

68. Marcq, E. *et al.* A latitudinal survey of CO, OCS, H_2O, and SO_2 in the lower atmosphere of Venus: Spectroscopic studies using VIRTIS-H. *J. Geophys. Res.* **113**, 2008JE003074 (2008).

69. Oschlisniok, J. *et al.* Sulfuric acid vapor and sulfur dioxide in the atmosphere of Venus as observed by the Venus Express radio science experiment VeRa. *Icarus* **362**, 114405 (2021).

70. Kolodner, M. A. & Steffes, P. G. The Microwave Absorption and Abundance of Sulfuric Acid Vapor in the Venus Atmosphere Based on New Laboratory Measurements. *Icarus* **132**, 151–169 (1998).

71. Krasnopolsky, V. Chemical kinetic model for the lower atmosphere of Venus. *Icarus* **191**, 25–37 (2007).

72. Young, A. T. Venus cloud microphysics. *Icarus* **56**, 568–577 (1983).

73. Palmer, K. F. & Williams, D. Optical Constants of Sulfuric Acid; Application to the Clouds of Venus? *Appl. Opt.* **14**, 208 (1975).

74. Tian, F. *et al.* Photochemical and climate consequences of sulfur outgassing on early Mars. *Earth and Planetary Science Letters* **295**, 412–418 (2010).

75. *CRC Handbook of Chemistry and Physics*. (CRC Press, 2016). doi:10.1201/9781315380476.

76. Toon, O. B. & Ackerman, T. P. Algorithms for the calculation of scattering by stratified spheres. *Appl. Opt.* **20**, 3657 (1981).

Methods

Cloud microphysics model

We have developed a 1D Venus cloud microphysics model to simulate the vertical profiles of cloud particles and condensational vapor species. The model used here is the Simulator of Particle Evolution, Composition, and Kinetics (SPECK)[51]. The model incorporates 45 size bins spanning from 1 nm to 30 μm, with the volume doubling from one bin to the next. The vertical domain extends from 40 km to 100 km altitudes with a 1 km interval. A central feature of SPECK is the implementation of a moving-center bin scheme to represent the particle size distributions[52]. This approach is designed to minimize numerical diffusion by treating particle growth in a Lagrangian manner within the size space for each bin. Using this scheme, SPECK has been shown to predict the size distribution with higher accuracy than existing models that calculate the particle growth in a Eulerian manner. Furthermore, SPECK is a highly versatile model, capable of handling multiple single-component, multicomponent and mixed particle size distributions, as well as their interactions. This capability allows for the assessment of complex particle composition evolution in the present study. These newly implemented schemes have been rigorously tested, validated against analytical solutions, and demonstrated to reproduce the observed Venus' cloud structure as measured by the PV LCPS[51].

We consider 3 condensational species (H_2SO_4, H_2O, and sulfur allotrope) and their homogeneous nucleation. We used photochemical model results[53] to incorporate the production of H_2SO_4 vapor at ~67 km, following recent cloud microphysics modeling[8]. Sulfur allotrope is generated as a result of the SO_2 photolysis[12,54]. We link its production rate to that of H_2SO_4 using a stoichiometric ratio from previous work[6–8]. Sulfur allotrope vapor consists of sulfur molecules with 2–10 atoms[55]. We assume the sulfur allotrope vapor is composed of S_8 because S_8 is the most stable and abundant form of sulfur allotrope under the thermal equilibrium in the temperature conditions of Venus' clouds[56]. The homogeneous nucleation of H_2SO_4 and H_2O is calculated based on the two-component nucleation parameterization[57], and S_8 homogeneous nucleation is calculated with classical homogeneous nucleation theory[1]. The saturation vapor pressure of S_8 vapor and the surface tension of condensed S_8, which is set to 72 mN m^{-1}, are taken from the nucleation experiment of sulfur allotrope[58].

MSPs are introduced as involatile particles composed of olivine ($FeMgSiO_4$) with a 1-nm radius[26,59,60]. The cosmic dust ablation model predicts that the peak ablation altitude of MSPs is

485 located at ~110 km[23], which is well above the model-top altitude of this study. Thus, we assume a
486 steady state MSP influx at the model-top altitude of 100 km, whose value is scaled by the cosmic
487 dust ablation rate. The cosmic dust ablation rate is not well constrained on Venus, while an ablation
488 model predicts it to be ~10 tons day^{-1} (ref.[23]). Based on this, we set the nominal cosmic dust
489 ablation flux to be 10 tons day^{-1} and conducted a parameter study ranging from 1 to 1000 tons
490 day^{-1}. It should be noted that the chemical form of iron compounds within H_2SO_4 droplets in the
491 Venusian atmosphere is still a subject of ongoing discussion. Ablated metals are expected to
492 initially form metal carbonates due to the high CO_2 density; these could then react with HCl, which
493 is also abundant above the clouds. Therefore, the resulting smoke particles may form from the
494 coagulation of metal chloride molecules. After these particles dissolve in cloud droplets and
495 subsequently evaporate below the cloud deck, the residual particles are likely metal sulfates.
496 However, since these details do not affect the main conclusion of this paper—that cosmic dust
497 ablation is the source of the haze—our model assumes a simplified MSP composition of olivine.
498 The cloud particles are divided into three distributions: solid distribution, H_2SO_4-H_2O
499 droplet distribution, and mixed distribution consisting of solid materials and H_2SO_4-H_2O. The solid
500 particle distribution corresponds to CCN particle distribution used in previous studies[6,9,20]. The
501 solid particles are composed of two kinds of materials: S_8 and MSP. Because S_8 has a low
502 saturation vapor pressure, it readily condenses onto MSP, resulting in two-component solid
503 particles. The homogenously nucleated S_8 particles are introduced to the smallest size bin of the
504 solid distribution, and H_2SO_4-H_2O particles to the H_2SO_4-H_2O droplet distribution. In addition,
505 the MSPs are introduced as solid particles at an injection altitude of 100 km. The solid particles
506 are allowed to grow via condensation of S_8 vapor and H_2SO_4 vapor. When S_8 vapor condenses on
507 the solid particles, these particles remain in the solid size distribution. When H_2SO_4 vapor
508 condenses on the solid particles, these solid particles are transferred to the mixed size distribution.
509 The rate of the conversion from solid particles to the mixed particles is calculated using
510 heterogeneous nucleation theory[61,62]. A contact parameter of unity (contact angle θ is set to 0°)
511 between the solid particles and H_2SO_4 liquid is assumed, given the absence of experimental data
512 on the contact angle of S_8 and MSPs against liquid H_2SO_4. We also assume that the mixed particles
513 do not grow via condensation of S_8 vapor once the solid particle is coated with H_2SO_4-H_2O liquid,
514 based on a previous study[63]. The mixed particles are also formed via coagulation between solid
515 particles and H_2SO_4-H_2O droplets. The coagulation rate is calculated as a sum of Brownian

516 diffusion and gravitational collection[1] for collisions of particles among solid, droplet, and mixed
517 particle distributions.
518 The background temperature and pressure are taken from the Venus International
519 Reference Atmosphere (VIRA)[64] (Extended Data Fig. 1a). The equatorial profiles are chosen for
520 comparison with past probe aerosol measurements since all of them landed in the equatorial region.
521 The Eddy diffusion profile is constructed based on a recent cloud microphysics model study[8],
522 which simultaneously reproduces Venus' cloud structure and condensational vapor profiles from
523 40 to 100 km (Extended Data Fig. 1b).
524 The bottom boundary conditions for vapor species are set to constant volume mixing ratios
525 (VMRs) at 40 km: 4 ppm for H_2SO_4, 30 ppm for H_2O, and 3.8 ppm for S_8. The VMRs of H_2SO_4
526 and H_2O are taken from previous observations[65–70], and the VMR of S_8 is taken from the
527 thermochemical model of Venus' lower atmosphere[71]. The bottom boundary conditions for
528 particle species are zero mixing ratio gradient, so their outward flux is determined by the
529 sedimentation flux. The upper boundary is closed for all vapor and particle species at 100 km,
530 except for the incoming MSP particles. The simulation is run for 1.5×10^{10} s (1500 Venus days),
531 which is long enough for the system to reach the steady state (Extended Data Fig. 2).
532
533 **Sensitivity studies**
534 We conducted three sensitivity studies to check the robustness of the conclusions of this
535 study, i.e., the lower haze particle formation driven by MSP influx.
536
537 **(i) Simulation without S_8 but including MSP influx**
538 We performed a simulation study that included MSP influx while excluding gaseous and
539 solid S_8. The purpose of this parameter study is to see whether the lower haze formation occurs
540 without the influence of S_8 particles. The assumed MSP influx is the nominal value (10 tons day^{-1}),
541 and only H_2SO_4 and H_2O are included as vapor species. Consequently, the particle formation is
542 mainly driven by the homogeneous nucleation of H_2SO_4-H_2O liquid in the upper haze region. The
543 results confirm that the lower haze formation occurs without the influence of S_8 (Extended Data
544 Fig. 3a and Extended Data Fig. 4a), reinforcing the robustness of the lower haze formation by the
545 MSP influx. However, this sensitivity study resulted in smaller cloud mass loading through all
546 altitudes (Extended Data Fig. 4b) due to the lack of S_8 CCN formation. This significant deviation

from the nominal case also affects the lower haze profile, making it narrower compared to the nominal case. Therefore, it is shown that the lower haze forms regardless of the presence of S_8 gas, but the shape of the distribution is influenced by the interaction with the main cloud.

(ii) Simulation under S_8 saturation

The VMR of S_8 vapor in the lower atmosphere is not observationally constrained. The lower haze particles can still be explained by S_8 particles if they can exist below the cloud deck. Such condition can be satisfied if S_8 vapor is saturated. Thus, we conducted a parameter study with saturated S_8 VMR at the bottom boundary and without including the MSP influx. Our simulation confirmed that the S_8 particles grow to a radius larger than 10 μm if S_8 vapor is saturated at the bottom boundary (Extended Data Fig. 3b and Extended Data Fig. 4a). The simulated size is too large to account for the observed lower haze particle size distribution. This indicates that the abundant S_8 vapor leads to increased condensation flux onto pre-existing particles. The enhanced condensation flux makes S_8 particles under the cloud bottom keep growing, instead of remaining in the sub-micron haze size distribution. This effect increases the mass loading under the cloud deck, which significantly deviates from the LCPS observation (Extended Data Fig. 4b).

(iii) Sensitivity to contact parameter

Although the contact angle between solid sulfur and liquid H_2SO_4 has not been experimentally measured, qualitative evidence suggests that sulfur is not easily wetted[72]. To test the robustness of our findings against this uncertainty, we performed a series of parameter studies using a wide range of contact angles (45˚, 90˚, 135˚, and 180˚). We found that the peak of the particle size distribution is almost completely insensitive to the chosen contact angle (Extended Data Fig. 5). While the total particle population remained similar across the simulations, the breadth of the size distribution showed slight variations at the smaller end. This indicates that the lower haze still forms with a consistent size distribution, regardless of the assumed wettability of the solid sulfur particles.

Abundances of involatile species in the lower haze

The abundances of olivine, Fe, Mg, and Si at 40 km are shown in Extended Data Table 1, within MSP influx range that reproduces the observed effective radius of the lower haze. The

abundances of Fe, Mg, and Si are derived directly from that of olivine based on the stoichiometry of $FeMgSiO_4$.

Calculation of extinction coefficient

We used Mie scattering theory to calculate the extinction coefficient of the aerosols. The refractive index of sulfuric acid was taken from Palmer & Williams[73], and the refractive index of S8 is taken from Tian et al[74]. As for the refractive index of MSP-derived materials, we use the value of metal sulfate to represent metal species that dissolve in the sulfuric acid droplets. The dominant components can be ferric sulfate or magnesium sulfate, whose refractive indices are reported to be 1.56 and 1.552 (ref. [75]), respectively. Accordingly, we adopted 1.56 to represent the refractive index of MSP-derived materials. For the mixed particles, we calculate the extinction coefficient assuming a core-shell structure[76] with sulfur allotrope core and sulfuric acid solution with metal sulfate inclusion, since the sulfur allotrope is likely insoluble in sulfuric acid[72].

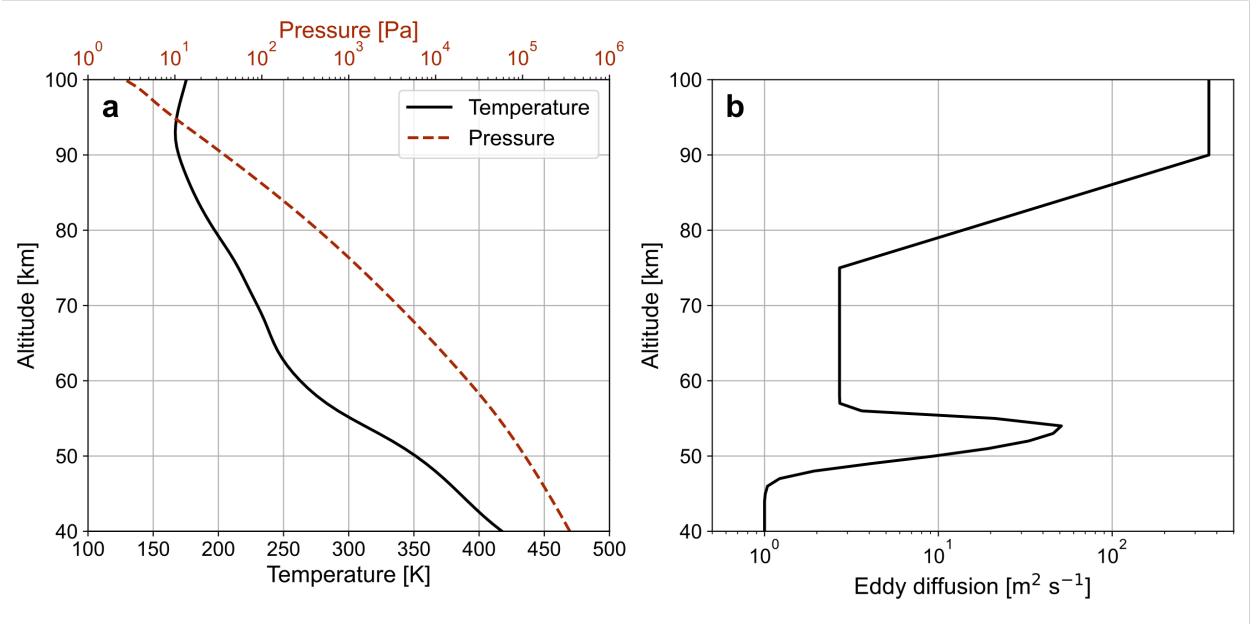

593

594 **Extended Data Fig. 1 | Atmospheric profiles used in this study. a**, temperature (black solid line)
595 and pressure (red dashed line) profiles used in this study, taken from VIRA equatorial profiles. **b**,
596 eddy diffusion profile used in this study.

597

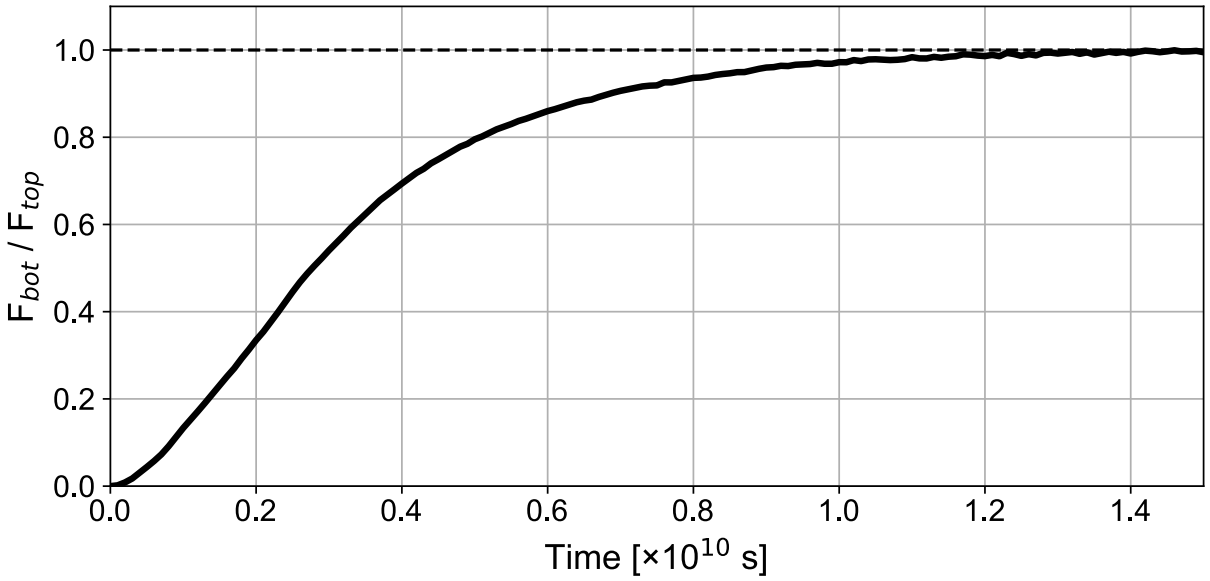

598

599 **Extended Data Fig. 2 | Evolution of olivine fluxes at the bottom and top of the model.** F_{bot}
600 indicates the olivine sedimentation flux at the bottom of the model, and F_{top} indicates the nominal
601 olivine flux as directly injected as MSP particles at the top of the model. The solid line represents
602 the ratio of F_{bot} to F_{top} , and the dashed line highlights the unity value ($F_{\mathrm{bot}}/F_{\mathrm{top}} = 1$) expected
603 at the steady state.

604

605

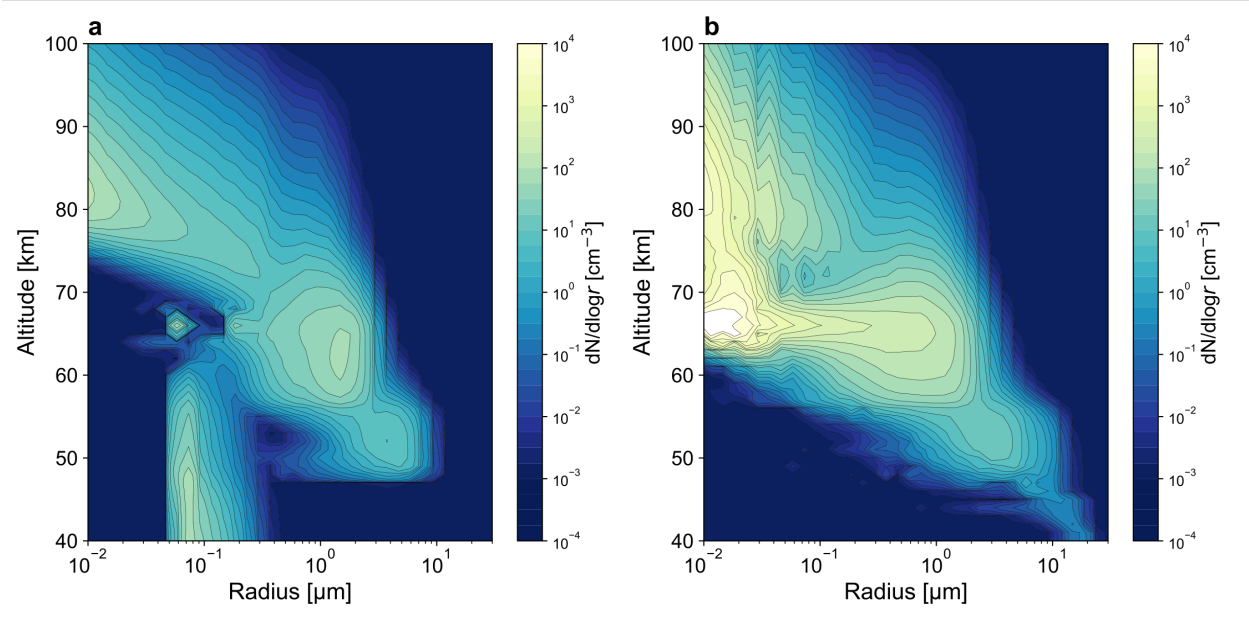

606

607 **Extended Data Fig. 3 | Size distribution in sensitivity study (i) and (ii). a, b,** Steady-state 2D
608 size distributions of aerosols as a function of particle radius (μm) and altitude (km) obtained from
609 the microphysics simulations (**a**) with MSP influx of 10 tons day^{-1} but without S_8 vapor, and (**b**)
610 with S_8 vapor abundance fixed at saturation VMR at the bottom boundary but without MSP influx.
611

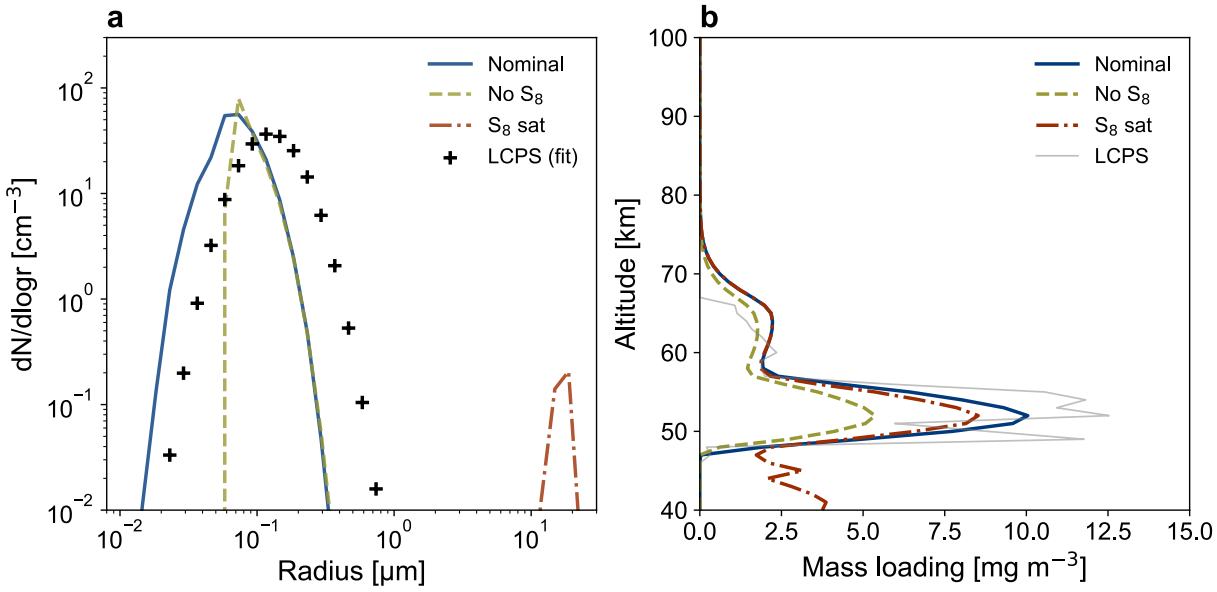

Extended Data Fig. 4 | Lower haze size distribution and mass loading profiles in sensitivity study (i) and (ii). (a) Steady-state size distributions of aerosols at 40 km as a function of particle radius (μm) obtained from microphysics simulations with the nominal settings (blue solid line), MSP influx of 10 tons day^{-1} but without S_8 vapor (yellow dashed line), and with S_8 vapor abundance fixed at saturation VMR at the bottom boundary but without MSP influx (red dash-dotted line). **(b)** Steady-state mass loading profiles as a function of altitude (km), obtained from microphysics simulations with the nominal settings (blue solid line), MSP influx of 10 tons day^{-1} but without S_8 vapor (yellow dashed line), and with S_8 vapor abundance fixed at saturation VMR at the bottom boundary but without MSP influx (red dash-dotted line). The LCPS results are also plotted for comparison in both panels.

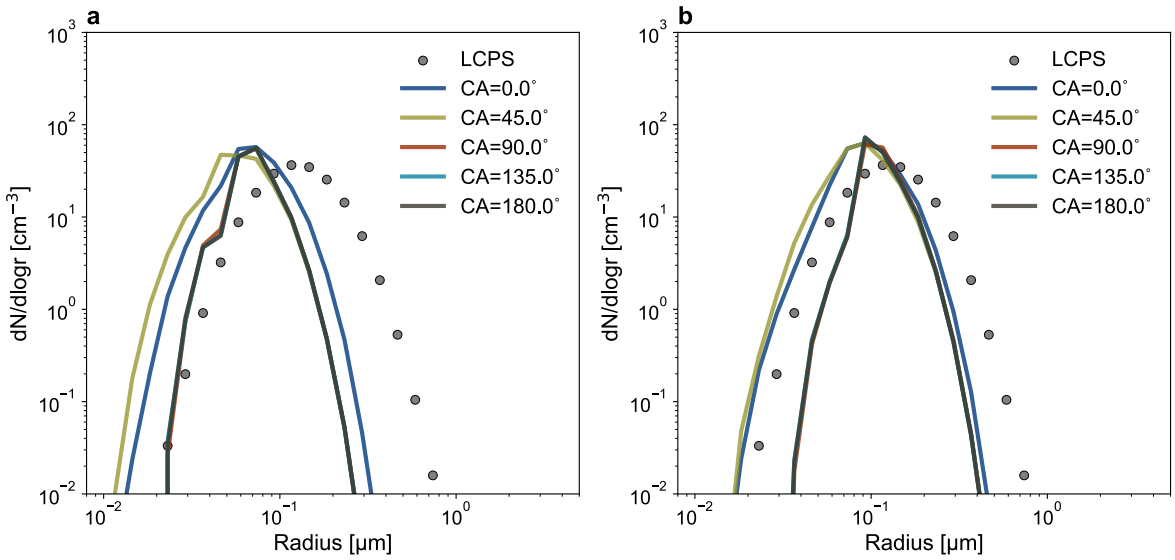

Extended Data Fig. 5 | Lower haze size distribution in sensitivity study (iii). a, Steady-state size distributions of aerosols at 40 km as a function of particle radius (μm) obtained from microphysics simulations using different contact angle (CA) ranging from 0˚ to 180˚ with an MSP flux of 10 tons day^{-1}. **b,** Steady-state size distributions of aerosols at 40 km as a function of particle radius (μm) obtained from microphysics simulations using different contact angle (CA) ranging from 0˚ to 180˚ with an MSP flux of 50 tons day^{-1}. The LCPS results are also plotted for comparison in both panels.

Extended Data Table 1 | The mass density of involatile species deposited as the lower haze particles at 40 km.

	Olivine (mg m^{-3})	Fe (mg m^{-3})	Mg (mg m^{-3})	Si (mg m^{-3})
5 tons day^{-1}	1.1×10^{-4}	3.0×10^{-5}	1.3×10^{-5}	1.5×10^{-5}
10 tons day^{-1}	1.7×10^{-4}	4.6×10^{-5}	2.0×10^{-5}	2.3×10^{-5}
20 tons day^{-1}	2.6×10^{-4}	7.2×10^{-5}	3.1×10^{-5}	3.6×10^{-5}
50 tons day^{-1}	4.6×10^{-4}	1.3×10^{-4}	5.5×10^{-5}	6.4×10^{-5}
100 tons day^{-1}	7.2×10^{-4}	2.0×10^{-4}	8.5×10^{-5}	9.8×10^{-5}

Data availability

The dataset that supports the findings of this study are available at https://doi.org/10.5281/zenodo.17456674.

Code availability

The code of SPECK is fully described by Karyu et al.[51] and archived at https://doi.org/10.5281/zenodo.14600375.

Methods references

51. Karyu, H. *et al.* A Microphysics Model of Multicomponent Venus' Clouds With a High-Accuracy Condensation Scheme. *Earth Space Sci.* **12**, e2025EA004203 (2025).
52. Jacobson, M. Z. *Fundamentals of Atmospheric Modeling,* 2nd edn (Cambridge UniversityPress, Cambridge, 2005).
53. Krasnopolsky, V. A. A photochemical model for the Venus atmosphere at 47–112km. *Icarus* **218**, 230–246 (2012).
54. Zhang, X., Liang, M. C., Mills, F. P., Belyaev, D. A. & Yung, Y. L. Sulfur chemistry in the middle atmosphere of Venus. *Icarus* **217**, 714–739 (2012).
55. Steudel, R., Steudel, Y. & Wong, M. W. Speciation and Thermodynamics of Sulfur Vapor. in *Elemental Sulfur and Sulfur-Rich Compounds I* (ed. Steudel, R.) vol. 230 117–134 (Springer Berlin Heidelberg, Berlin, Heidelberg, 2003).
56. Lyons, J. R. An estimate of the equilibrium speciation of sulfur vapor over solid sulfur and implications for planetary atmospheres. *J. Sulfur Chem.* **29**, 269–279 (2008).
57. Määttänen, A. *et al.* New Parameterizations for Neutral and Ion-Induced Sulfuric Acid-Water Particle Formation in Nucleation and Kinetic Regimes. *J. Geophys. Res.***123**, 1269–1296 (2018).

58. Onischuk, A. A. *et al.* Surface tension of sulfur nanoparticles as determined from homogeneous nucleation experiments. *J. Aeros. Sci.* **97**, 1–21 (2016).

59. Saunders, R. W. & Plane, J. M. C. A laboratory study of meteor smoke analogues: Composition, optical properties and growth kinetics. *J. Atmos. Sol.-Terr. Phys.* **68**, 2182–2202 (2006).

60. Frankland, V. L. *et al.* CO oxidation and O2 removal on meteoric material in Venus' atmosphere. *Icarus* **296**, 150–162 (2017).

61. Inada, A. Simulations of Martian surface fog and calibration of Mars Imaging Camera for its future observations. (Kobe University, Kobe, Japan, 2002).

62. Määttänen, A. *et al.* Nucleation studies in the Martian atmosphere. *J. Geophys. Res.* **110**, 2004JE002308 (2005).

63. Toon, O. B., Turco, R. P. & Pollack, J. B. The ultraviolet absorber on Venus: Amorphous sulfur. *Icarus* **51**, 358–373 (1982).

64. Seiff, A. *et al.* Models of the structure of the atmosphere of Venus from the surface to 100 kilometers altitude. *Adv. Space Res.* **5**, 3–58 (1985).

65. Arney, G. *et al.* Spatially resolved measurements of H_2O, HCl, CO, OCS, SO_2, cloud opacity, and acid concentration in the Venus near-infrared spectral windows: MEASUREMENTS OF VENUS LOWER ATMOSPHERE. *J. Geophys. Res.* **119**, 1860–1891 (2014).

66. Bézard, B., Fedorova, A., Bertaux, J.-L., Rodin, A. & Korablev, O. The 1.10- and 1.18-μm nightside windows of Venus observed by SPICAV-IR aboard Venus Express. *Icarus* **216**, 173–183 (2011).

682 67. Fedorova, A., Bézard, B., Bertaux, J.-L., Korablev, O. & Wilson, C. The CO2 continuum
683 absorption in the 1.10- and 1.18-μm windows on Venus from Maxwell Montes transits by
684 SPICAV IR onboard Venus express. *Planet. Space Sci.* **113–114**, 66–77 (2015).
685 68. Marcq, E. *et al.* A latitudinal survey of CO, OCS, H_2O, and SO_2 in the lower atmosphere of
686 Venus: Spectroscopic studies using VIRTIS-H. *J. Geophys. Res.* **113**, 2008JE003074 (2008).
687 69. Oschlisniok, J. *et al.* Sulfuric acid vapor and sulfur dioxide in the atmosphere of Venus as
688 observed by the Venus Express radio science experiment VeRa. *Icarus* **362**, 114405 (2021).
689 70. Kolodner, M. A. & Steffes, P. G. The Microwave Absorption and Abundance of Sulfuric Acid
690 Vapor in the Venus Atmosphere Based on New Laboratory Measurements. *Icarus* **132**, 151–
691 169 (1998).
692 71. Krasnopolsky, V. Chemical kinetic model for the lower atmosphere of Venus. *Icarus* **191**, 25–
693 37 (2007).
694 72. Young, A. T. Venus cloud microphysics. *Icarus* **56**, 568–577 (1983).
695 73. Palmer, K. F. & Williams, D. Optical Constants of Sulfuric Acid; Application to the Clouds
696 of Venus? *Appl. Opt.* **14**, 208 (1975).
697 74. Tian, F. *et al.* Photochemical and climate consequences of sulfur outgassing on early Mars.
698 *Earth Planet. Sci. Lett.* **295**, 412–418 (2010).
699 75. *CRC Handbook of Chemistry and Physics*. (CRC Press, 2016).
700 76. Toon, O. B. & Ackerman, T. P. Algorithms for the calculation of scattering by stratified
701 spheres. *Appl. Opt.* **20**, 3657 (1981).

702

703 **Acknowledgements**

704 This study was supported by the Japan Society for the Promotion of Science (JSPS)
705 (KAKENHI Grants JP22H00164, JP23KJ0201, JP23K25932, JP24K21561, and JP25K01051),

JST FOREST Program (Grant JPMJFR212U, Japan), and the International Joint Graduate Program in Earth and Environmental Sciences (GP-EES) of Tohoku University. We thank M. Luginin for providing the aerosol extinction data derived from the SPICAV-IR instrument onboard VEx.

Author contributions

H.K. conceptualized the study, developed the model, performed the simulations and analysis, and wrote the original draft. **T.K., Ann.M., Arn.M.,** and **S.V.** contributed to the development and validation of the model. **Ann.M.** also provided specialized insights into cloud microphysics and nucleation processes. **N.T., S.R., A.C.V.,** and **M.C.** provided supervision for the project. All authors contributed to the writing and editing of the manuscript.

Competing interests

The authors declare no competing interests.

Additional information

None